Lawrence Berkeley National Laboratory
Recent Work

Title
Chemical forms of calcium in Ca,Zn- and Ca,Cd-containing grains excreted by tobacco trichomes

Permalink
https://escholarship.org/uc/item/9jc85075

Journal
Canadian Journal of Chemistry, 85

Authors
Sarret, Geraldine
Isaure, Marie-Pierre
Marcus, Matthew A.
et al.

Publication Date
2007-10-01

Chemical forms of calcium in Ca,Zn- and Ca,Cd-containing grains

excreted by tobacco trichomes

Géraldine Sarret[1], Marie-Pierre Isaure, Matthew A. Marcus, Emiko Harada,

Yong-Eui Choi, Sébastien Pairis, Sirine Fakra and Alain Manceau

Géraldine Sarret, Marie-Pierre Isaure, Emiko Harada and Alain Manceau. Environmental Geochemistry Group, LGIT, University of Grenoble and CNRS, BP 53, 38041 Grenoble cedex 9, France

Matthew A. Marcus and Sirine Fakra. Advanced Light Source (ALS), Lawrence Berkeley National Lab, MS 6-100, Berkeley, CA 94720, USA

Emiko Harada and Yong-Eu Choi. Division of Forest Resources, College of Forest Sciences, Kangwon National University, Chunchon 200-701, Kangwon-do, Korea

Sébastien Pairis. Institut Néel CNRS-UJF, Dept. Matière Condensée, Matériaux et Fonctions, Pôle Instrumentation (Microscopie Electronique), 25 av. des Martyrs, BP 166, 38042 Grenoble cedex 9, France

[1] Corresponding author. Email: geraldine.sarret@ujf-grenoble.fr

Tel: (33) 4 76 82 80 21, Fax: (33) 4 76 82 81 01

Abstract

Tobacco (*Nicotiana tabacum* L. cv. Xanthi) plants exposed to toxic levels of zinc and cadmium

excrete metals through their leaf trichomes (epidermal hairs) as Zn,Ca- and Cd,Ca-containing

grains. Little is known about the nature and formation mechanism of these precipitates. The

chemical, crystalline, and non-crystalline compositions of individual grains produced by tobacco

were studied by scanning electron microscopy coupled with energy dispersive X-ray analysis

(SEM-EDX), micro-X-ray diffraction (μXRD) and calcium K-edge micro X-ray absorption near

edge structure (μXANES) spectroscopy. Zinc is predominantly incorporated in calcite, and

cadmium in calcite and vaterite. Aragonite, which occurs occasionally, does not seem to contain

trace metals. In addition to being precipitated in its three possible polymorphic forms, calcite,

aragonite and vaterite, calcium also is speciated as amorphous $CaCO_3$ and possibly organic Ca in

some grains. Most often, a particular grain consists of two or more crystalline and non-crystalline

phases. The observed variability of intra- and inter-grain elemental and phase composition

suggests that this biomineralization process is not constrained by biological factors, but instead

results from thermodynamically and kinetically controlled reactions. This study illustrates the

potential of laterally resolved X-ray synchrotron radiation techniques (μXRD and μXANES) to

study biomineralization and metal immobilization processes in plants.

Introduction

20 Recently, a novel original mechanism of Zn and Cd detoxification was described in tobacco

21 (*Nicotiana tabacum* L. cv. Xanthi). Tobacco exposed to Cd excreted Cd,Ca-containing grains

22 through leaf trichomes (1, 2), and a similar excretion of Zn,Ca-containing grains was observed

23 under Zn exposure (3). Trichomes are specialized epidermal structures. In tobacco, they are

24 glandular and excrete various organic substances including nicotine and resins. Such

25 detoxification process may have implication in human health since smoking is one of the

26 principal routes of exposure to heavy metals, and also in phytoremediation as tobacco is a

27 candidate species for phytoextraction.

28 The morphology, elemental composition, mineralogy as well as Zn and Cd speciation in the

29 grains were investigated by scanning electron microscopy coupled with energy dispersive X-ray

30 analysis (SEM-EDX), micro-X-ray fluorescence (μXRF), micro-X-ray diffraction (μXRD), Zn

31 K-edge micro extended X-ray absorption fine structure (μEXAFS) (3) and Cd L_{III} edge micro X-

32 ray absorption near edge structure (μXANES) spectroscopy (Isaure et al., in prep.). Calcium was

33 always the major component. μXRD analyses revealed the presence of calcite, and less

34 frequently vaterite and aragonite, two other $CaCO_3$ polymorphs. Calcium oxalate mono and

35 dihydrate were found occasionally. Calcite and vaterite were substituted by cations, probably Zn,

36 Cd and possibly Mn and Mg. Zn μEXAFS confirmed the occurrence of Zn-substituted calcite,

37 and evidenced Zn associations with other phases including organic compounds, silica and

38 phosphate (3). Cd μXANES showed that cadmium was a Ca substituent in calcite and vaterite

39 and/or sorbed on the surface of these minerals (Isaure et al., in prep.).

40 The mechanism of formation of these grains remains unclear. Biogenic minerals may result from

41 a controlled biomineralization process leading to well defined minerals and shapes. They may

42 also be "biologically induced", which means that an organism promotes the precipitation, but

3

43 does not control the crystallization process (4). In the present case, grains could result from the

44 exudation of a liquid containing the various metals and substances, and precipitation of the

45 various solid phases due to water evaporation. Alternatively, they might be formed intracellularly

46 and excreted thereafter as suggested by Choi et al. (5). The purpose of this study is to better

47 characterize the structure and composition of the grains. Grains excreted by tobacco under

48 various Zn, Cd and Ca exposure conditions were investigated by SEM-EDX, µXRD and Ca K-

49 edge µXANES spectroscopy. Results of these complementary approaches are compared, and a

50 hypothesis for the formation of the grains is proposed in light of these data.

51

52 **Experimental**

53 *Materials*

54 Plant culture and grain collection procedure have been described previously (3). Briefly, tobacco

55 plants were grown in hydroponic conditions and exposed for 5 weeks to Zn or Cd, with or

56 without a supplement of Ca (Table 1). A control condition with Ca only was also tested. Then,

57 grains were collected by washing the leaves in ultrapure water and centrifugating the suspension.

58 Several Ca-containing reference compounds were used for the Ca XANES data analysis.

59 Calcite, vaterite and Cd-containing vaterite were synthesized at room temperature according to a

60 modified protocol of Paquette and Reeder (6, 7). Briefly, an aqueous solution (500 mL)

61 containing 10 mM $CaCl_2$ and 1.8 M NH_4Cl was placed in a glass reactor, an EPPENDORF tube

62 containing solid ammonium carbonate was allowed to float at the surface of the solution, and the

63 reactor was closed and kept unstirred. NH_4Cl was used as a background electrolyte to provide a

64 high ionic strength. Initial pH was 4.9. The decomposition of ammonium carbonate produces

65 $NH_3(g)$ and $CO_2(g)$, which dissolve into the solution, simultaneously increasing pH and

66 alkalinity. The supersaturation of the solution induces the formation and growth of $CaCO_3$

67   crystals. Continuous sublimation of $NH_3(g)$ buffers the solution around pH = 7.9. After 13 days,

68   the reactor contained rhombohedral crystals and spherical particles attached on the surface of the

69   glass. The two types of particles were separated and characterized by XRD. Rhombohedral

70   crystals corresponded to calcite, and spherical particles to vaterite. For the synthesis of Cd-

71   containing vaterite, the same procedure was used except that after 13 days, when crystal size

72   amounted to 150-200 μm in diameter, the $CaCl_2$-NH_4Cl solution was progressively doped with

73   0.1 M $CdCl_2$ to a total concentration of 100 μM Cd in order to incorporate Cd as a Ca substituent

74   in vaterite (6, 7). The progressive addition of $CdCl_2$ kept the solution undersaturated with respect

75   to otavite ($CdCO_3$). After 7 days, the particles were collected and separated. Spherical particles

76   were identified as Cd-containing vaterite by XRD and μXRF. The Cd content was a few tens

77   ppm based on μXRF analysis.

78   Aragonite was a natural specimen. The XANES spectrum for synthetic amorphous $CaCO_3$ was

79   provided by Y. Politi (8). Ca oxalate monohydrate (whewellite) was purchased from Aldrich. A

80   solution containing 0.5 M $Ca(NO_3)_2$ at pH 2.6 was used as a reference for aqueous Ca^{2+}. The

81   phase purity of all crystalline samples was checked by XRD prior to XANES analysis.

82

83   *Electron microscopy*

84   The morphology and the chemical composition of the grains were studied by SEM-EDX using a

85   Jeol-JSM 840A equipped with a Kevex Si(Li) detector. The chamber pressure was 10^{-6}-10^{-5} Torr,

86   and the accelerating voltage 20 kV. Grains were mounted on kapton tape or on carbon tape, then

87   fixed on carbon stubs and coated with carbon. Images were taken at a magnification of 500 to

88   10000. EDX spectra were recorded on prominent spots of the grains to optimize the detection.

89

90   *Micro-XRF, μXRD and μXANES*

91   The μXRF, μXRD and Ca K-edge μXANES measurements were performed on beamline 10.3.2

92   of the Advanced Light Source (ALS, Berkeley, CA) (9). The grains were spread on kapton tape

93   and analyzed at room temperature and pressure. First, each grain was mapped by μXRF. Then,

94   μXANES and μXRD and data were recorded on the Zn-richest region for the Zn and Zn + Ca

95   treatments, on the Cd-richest region for the Cd and Cd + Ca treatment, and on the Ca-richest

96   region for the Ca treatment. μXRF data were collected at 10 keV with a beam size of 5×5 μm.

97   The same X-ray spot size was used for Ca μXANES. Fluorescence X-ray yield was measured

98   with a 7-element Ge solid-state detector. The spectra were recorded between 3900 to 4400 eV.

99   μXRD patterns were recorded at an incident energy of 17 keV with a beam size of 16×7 μm.

100 More experimental details are given in (3). Ca XANES reference spectra were recorded at room

101 temperature on beamline ID21 at the European Synchrotron Radiation Facility (ESRF, Grenoble,

102 France). Each spectrum is the average of two to three spectra, each about 15 minutes long.

103

104 *XRD and XANES data treatment*

105 The XRD data treatment was performed as described previously (3). Briefly, after calibration with

106 alumina, two dimensional XRD patterns were integrated to one-dimensional patterns for peak

107 assignment. For substituted calcite crystals, the unit cell parameters *a* and *c* were refined, and the

108 stoichiometry of the substituent was estimated from these two parameters using the Vegard law

109 (10) with calcite, smithsonite ($ZnCO_3$) and otavite ($CdCO_3$) as end-members for the Ca-Zn and Ca-

110 Cd solid solutions. This approach cannot be used for substituted vaterite because of the absence of

111 a $CdCO_3$ structural analogue of vaterite.

112 XANES spectra were processed using WinXAS (11). All spectra were energy calibrated

113   with respect to calcite (inflection point for this reference set to 4042.6 eV). The collected scans

114   were averaged; background subtracted and normalized using linear (pre-edge) or cubic (post-

115   edge) polynomials. XANES spectra were then fitted by linear combinations using calcite,

116   aragonite, vaterite, Cd-containing vaterite, amorphous $CaCO_3$, aqueous Ca^{2+} and Ca oxalate

117   monohydrate reference spectra. The quality of the fits was quantified by the normalized sum-

118   squares residuals $NSS = \Sigma(\mu_{experimental} - \mu_{fit})^2 / \Sigma(\mu_{experimental})^2 \times 100$, in the 4000-4150 eV

119   range, where μ is the normalized absorbance. An energy shift of ± 0.5 eV maximum and a

120   correction of slope were allowed to account for the energy resolution of the monochromator and

121   for possible inconsistencies in data processing. For some spectra, linear combination (LC) fitting

122   did not provide satisfactory results, and over-absorption effects were suspected based on the

123   comparison of these spectra with the standards. Therefore, each spectrum was fitted with and

124   without a correction of over-absorption using a simple model (12). This model assumes that the

125   smooth part of the resonant absorption is a constant fraction of the non-resonant background

126   (which is a reasonable assumption in the XANES region) and that the sample is infinitely thick,

127   *i.e.*, totally absorbs the incident beam (which is probably true considering the energy range and

128   the size and global composition of the grains). The equation used is:

129        $y_{experimental} = (1 + a) / (1 + a \cdot y_{corrected})$ (1)

130   where y is the normalized resonant absorbance, which equals 0 below the edge and

131   oscillates around 1 above the edge, and $a = \mu_{resonant} / (\mu_{non\ resonant} + \mu_{fluorescence})$

132   where $\mu_{resonant}$, $\mu_{non\ resonant}$ and $\mu_{fluorescence}$ are the three components of the absorbance μ.

133   Equation (1) can be solved as:

134        $y_{corrected} = y_{experimental} / (1 + a (1 - y_{experimental}))$ (2)

7

135   The over-absorption parameter *a* equals 0 in the absence of over-absorption effect, and

136   increases with this effect. Because of the sample heterogeneity, the precise composition of the

137   sample is not known, so *a* is an adjusted parameter.

138

139   **Results**

140   The morphology of the grains as observed by SEM varied considerably. The grains varied from

141   10 μm to 150 μm in diameter. Each grain is an aggregate of different types of particles. The first

142   type is micro faceted crystallites (Insets in Fig. 1a and 1b) and the second type is globular

143   structures of various sizes (from 2 to 50 μm, Fig. 1c, 1d and 1e). Some grains such as Zn2 (Fig.

144   1c) seem visually less crystalline. The elemental composition of the grains varies from one grain

145   to another, and within the same grain. Ca was always the major component regardless of the plant

146   metal treatment conditions. Minor elements include Mg, Si, P, Cl, K, and Zn or Cd depending on

147   the plant treatment (Fig. 1). The high Si peaks observed in Fig. 1a to 1d are attributed to kapton

148   tape on which the grains were mounted. Silicon is not detected in the grain presented in Fig. 1e

149   (mounted on carbon tape). However, Si was found in small amount in some grains (not presented

150   in this study), as well as Mn.

151   Our previous study using μXRD (3) showed that grain ZnCa3 contained substituted calcite and

152   aragonite, that grain ZnCa4 contained substituted calcite, and that grain Zn2 did not contain

153   crystalline phases. The two-dimensional μXRD patterns for grains ZnCa5 and Zn3 show that the

154   Bragg reflections for these two grains consist of small arcs of Debye-Scherrer rings, indicating

155   that the grains are composed of micrometer-size mosaic crystals (Fig. 2b). All reflections

156   correspond to substituted calcite, and the major Ca substituent is Zn based on μXRF (Fig. 2a).

157   Note that although Ca is the major element, the Ca Kα peak has a low intensity relative to the Zn

158   Kα peak due to air absorption and the lower fluorescence yield of Ca *vs*. Zn. The refined unit cell

159   parameters a and c for grain ZnCa5 and Zn3 were 4.97 and 16.97 Å, and 4.95 and 16.83 Å,

160   respectively, compared to 4.9896 and 17.0610 Å for pure calcite. The calculated formulae using

161   the Vegard law were $Ca_{0.95}Zn_{0.05}CO_3$ and $Ca_{0.89}Zn_{0.11}CO_3$, respectively. The difference in the Zn

162   stoichiometry coefficient obtained using parameters a and c was ± 0.01. The µXRD results for

163   the Cd-containing grains will be presented separately together with Cd L_{III}-XANES data (Isaure

164   et al., in preparation). Briefly, the grains CdCa2 and Cd10 contain micrometer crystals of

165   substituted calcite and finer (nanometer sized) crystals of substituted vaterite. Grain CdCa3

166   contains nano-crystals of substituted vaterite only. Finally, no crystalline phases were detected in

167   grain CdCa6. For Cd- substituted calcite, the Vegard law provides an imprecise estimation of Cd

168   stoichiometry because the contrast in ionic radius between Cd and Ca is small (0.95 Å for Cd^{2+}

169   and 1.00 Å for Ca^{2+} compared to 0.74 Å for Zn^{2+}) (13). For instance, the substitution rate for

170   grain CdCa2 could be anywhere between 30 and 80%. It was not possible to calculate the

171   stoichiometry of Cd in vaterite because of the absence of a Cd end member (see the Experimental

172   section).

173   Calcium being the major element in the grains, Ca K-edge µXANES spectroscopy was then

174   performed to get some insights on the composition of the grains, and test for the presence of

175   amorphous Ca phases. Figure 3a shows the XANES spectra for several Ca reference compounds.

176   The four $CaCO_3$ species (calcite, vaterite, aragonite and amorphous $CaCO_3$ (ACC)) have clearly

177   distinct spectra, which enables their identification (14, 15). However, Ca XANES has no

178   sensitivity to substitutional impurities as seen for instance for low Cd-containing vaterite (Cd

179   content lower than 1%, as estimated by µXRF) and pure vaterite exhibiting nearly identical

180   spectra. The spectra for aqueous Ca^{2+}, Ca oxalate monohydrate and ACC share some similarities.

181   However, the lower part of the edge is shifted to lower energy for ACC spectrum, and the

182   maximum of the white line (zero value of the first derivative) increases from 4049.5 eV (ACC) to

183   4049.9 eV (Ca oxalate monohydrate) and to 4050.5 eV (aqueous Ca^{2+}, Fig. 3b). The aragonite

184   spectrum is distinct from the three previous spectra in displaying a shoulder at 4046 eV (arrow in

185   Fig. 3), and a minimum between 4060 and 4070 eV.

186   Figure 4 shows the Ca μXANES spectra for the grains. They were fitted by LC using the standard

187   spectra presented above, and results are presented in Table 2. The ZnCa3 spectrum presents

188   strong similarities with the aragonite spectrum, but markedly lower amplitude. The drop in

189   amplitude suggests some over-absorption effect (12) due to a high Ca content of the analyzed

190   spot. The fit without over-absorption correction (see materials and Methods) did not provide

191   satisfactory result (NSS = 0.065 %, with 68% vaterite + 25% aragonite). Introducing an over-

192   absorption correction greatly improved the fit (NSS = 0.014 % with aragonite as only component,

193   Fig. 4). The a value found (1.38) corresponds to a very strong over-absorption effect. The fit was

194   not improved significantly by introducing a second component (NSS decreased by less than

195   10%). Thus, the spot analyzed by μXANES likely contains aragonite as the sole Ca species.

196   The grains ZnCa4 and ZnCa5 were fitted with 98% calcite. The fit was slightly improved with a

197   correction of over-absorption (NSS = 0.015 and 0.021 %, compared to 0.020 and 0.035 %,

198   respectively), and the proportions were unchanged. Adding a second component did not improve

199   significantly the fits (NSS decreased by less than 10%).

200   For grain Zn2 and CdCa6, fits without over-absorption correction were not satisfactory (NSS =

201   0.048 and 0.091 %, respectively, for two-component fits). Fair one-component fits with over-

202   absorption correction were obtained with ACC (NSS = 0.021 and 0.024 %, respectively), but the

203   match was not optimal for the first oscillation (around 4080 eV). Ca oxalate monohydrate and

204   aqueous Ca^{2+} provided weaker fits (NSS = 0.086 and 0.053 % for Zn2, and 0.076 and 0.043 % for

205   CdCa6, respectively). Adding a second component did improve the reproduction of the first

206   oscillation. Several fits of equivalent qualities were obtained with ACC as major component

207 (about 80 and 70 % of total Ca) and various species as secondary component. *NSS* values were

208 more than doubled if ACC was excluded (Table 2 and Fig. 1 in Supplemental Information).

209 Therefore, grains Zn2 and CdCa6 likely contain ACC as major species, and an additional species

210 whose nature remains unknown.

211 For the other grains (Zn3, CdCa2, CdCa3 and Cd10), over-absorption correction did not improve

212 the fits. Calcite was the major form in grains Zn3 and CdCa2, and fits of equivalent quality were

213 obtained with ACC, aqueous Ca^{2+} and Ca oxalate monohydrate as minor species. Aqueous Ca^{2+}

214 is unlikely in solid-state material. ACC and Ca oxalate monohydrate are more likely. In the

215 absence of reference spectra for Ca bound to organic ligands other than oxalate, this latter

216 compound may be considered as a proxy for Ca bound to organic compounds in general.

217 Therefore, this pool is referred to as "organic Ca and/or ACC" in Table 3. Vaterite was found in

218 grains CdCa3 and Cd10. For this latter grain only, no satisfactory fit was obtained with two

219 components (*NSS* = 0.046 %), so a third component was introduced. Again, a contribution of

220 organic Ca and/or ACC was found in grains CdCa3 and Cd10.

221

222 The speciation of Ca was then compared with the mineralogy and morphology of the grains

223 (Table 3). The percentages were rounded to the nearest ten for clarity. Except for two grains,

224 ZnCa3 and CdCa2, the same crystalline species were identified by μXRD and Ca μXANES. Zn-

225 substituted calcite and Cd-substituted vaterite were identified by μXRD in grains ZnCa3 and

226 CdCa2, respectively, but not by Ca μXANES spectroscopy. This difference likely results from

227 the larger beam size and higher penetration depth of X-rays in XRD measurements relative to

228 μXANES (16×7 μm *vs* 5×5 μm, and a few tens of μm at 17 keV *vs*. a few μm at 4 keV). Thus,

229   XRD probes a different material volume than Ca µXANES even when conducted on the same

230   spot.

231

232   **Discussion and Conclusion**

233   Results showed that beside crystalline calcium carbonates (calcite, vaterite and aragonite), the

234   tobacco grains contained ACC as well. Whewellite (Ca oxalate monohydrate) did show up in

235   some XANES fits, but its presence could not be firmly attested. Ca oxalate mono- and dihydrate

236   have several XRD peaks in common with calcite, but peaks at distinct positions as well. These

237   two minerals were positively identified by µXRD in other tobacco grains based on the presence

238   of these specific peaks (3). In the present study, no such peaks were found on the XRD patterns.

239   However, it is still possible that coarse crystals of Ca oxalate mono or dihydrate are present but

240   produce non-specific peaks only, or that Bragg conditions were not met for these coarse crystals.

241   Therefore, the presence of Ca oxalate mono- and dihydrate cannot be ruled out. Other

242   undetermined organic ligands may also complex Ca. In addition, mixed mineral and organic Ca

243   compounds such as organic matter-containing calcite (16) may occur.

244   The Ca µXANES analysis showed that strong over-absorption effects may take place and

245   decrease dramatically the amplitude of the spectra. We show that this effect is far from negligible

246   when identifying and quantifying Ca species. For instance, for grain ZnCa3, the uncorrected

247   spectrum was fitted by 68% vaterite + 25% aragonite, and the corrected spectrum was fitted with

248   100% aragonite. Note that the LCF without over-absorption correction was relatively bad, which

249   alerted us on the possibility of an over-absorption effect.

250   In the environment, ACC is thermodynamically unstable and rapidly transforms into vaterite and

251   then calcite (17). However, it is found as a stable compound in plants (e.g., cystoliths) and

252   animals (e.g., cuticle of crustaceans, spicules of ascidiae, granules in molluscs) (18). ACC is

253 probably stabilized by proteins, magnesium and phosphorus in these organisms (18). In our case,

254 Mg and P were found in the grains.

255 Biologically controlled biomineralization leads to well defined mineral species and shapes.

256 Here, the variety of morphologies and of $CaCO_3$ crystal structures, and their coexistence with

257 amorphous and possibly organic forms, supports the hypothesis of a biologically induced (as

258 opposed to biologically controlled) biomineralization. This study illustrates the potential of

259 microfocused X-ray techniques to study biomineralization processes, and strategies of metals

260 immobilization developed by plants to cope with metal toxicity.

261

References

1.   Choi, Y. E., Harada, E., Wada, M., Tsuboi, H., Morita, Y., Kusano, T. & Sano, H. Planta **213**, 45-50 (2001).

2.   Choi, Y. E., Harada, E., Kim, G. H., Yoon, E. S. & Sano, H. J. Plant Biol. **47**, 75-82 (2004).

3.   Sarret, G., Harada, E., Choi, Y. E., Isaure, M. P., Geoffroy, N., Birschwilks, M., Clemens, S., Fakra, S., Marcus, M. A. & Manceau, A. Plant Physiol. **141**, 1021-1034 (2006).

4.   Lowenstam, H. & Weiner, S. On Biomineralization (Oxford University Press, New York, Oxford, 1989).

5.   Choi, Y. E. & Harada, E. J. Plant Biol. **48**, 113-119 (2005).

6.   Paquette, J. & Reeder, R. J. Geochim. Cosmochim. Acta **59**, 735–749 (1995).

7.   Reeder, R. J. Geochim. Cosmochim. Acta **60**, 1543–1552 (1996).

8.   Politi, Y., Levi Kalisman, Y., Raz, S., Wilt, F., Addadi, L., Weiner, S. & Sagi, I. Adv. Funct. Mat. **16**, 1289-1298 (2006).

9.   Marcus, M. A., MacDowell, A. A., Celestre, R., Manceau, A., Miller, T., Padmore, H. A. & Sublett, R. E. J. Synchrotron Rad. **11**, 239-247 (2004).

10.   West, A. Solid State Chemistry and its Applications (Wiley, New York, 1984).

11.   Ressler, T. J. Phys. IV **7**, c2-269 (1997).

12.   Manceau, A., Marcus, M. A. & Tamura, N. in Applications of Synchrotron Radiation in Low-Temperature Geochemistry and Environmental Science (eds. Fenter, P., Rivers, M., Sturchio, N. & Sutton, S.) 341-428 (Reviews in Mineralogy and Geochemistry, Mineralogical Society of America, Washington, DC., 2002).

13.   Shannon, R. D. Acta Crystallogr. A **32**, 751-767 (1976).

14.   Levi Kalisman, Y., Raz, S., Weiner, S., Addadi, L. & Sagi, I. Adv. Funct. Mat. **12**, 43-48 (2002).

15.   Pattanaik, S. Nucl. Inst. Meth. Phys. Res. B **229**, 367-374 (2005).

16.   Phillips, B. L., Lee, Y. J. & Reeder, R. J. Environ. Sci. & Technol. **39**, 4533-4539 (2005).

17.   Ogino, T., Suzuki, T. & Sawada, K. J. Cryst. Growth **100**, 159-67 (1990).

18.   Weiner, S., Levi Kalisman, Y., Raz, S. & Addadi, L. Connective Tissue Research **44 Suppl. 1**, 214-218 (2003).

Table 1. Tobacco culture conditions and name of the grains investigated

Treatment conditions	Cation Concentrations in the Nutrient Solution (mM)			Grain Names	Techniques and References				
	Ca	Zn	Cd		SEM-EDX	μXRD	Zn μEXAFS	Cd μXANES	Ca μXANES
Zn	0.28	0.25	0	Zn2	(3) and this paper	(3)	(3)	-	this paper
				Zn3	-	this paper	unpubl.	-	
Zn + Ca	3.28	0.25	0	ZnCa3	(3) and this paper	(3)	(3)	-	this paper
				ZnCa4	(3) and this paper	(3)	(3)	-	this paper
				ZnCa5	-	this paper	unpubl.	-	this paper
Cd	0.28	$0.08 \cdot 10^{-3}$	0.025	Cd10	(a)	(a)	-	(a)	this paper
Cd + Ca	3.28	$0.08 \cdot 10^{-3}$	0.025	CdCa2	(a)	(a)	-	(a)	this paper
				CdCa3	(a)	(a)	-	(a)	this paper
				CdCa6	(a)	(a)	-	(a)	this paper
Ca	3.28	$0.08 \cdot 10^{-3}$	0	Ca3	this paper	-	-	-	-

(a) Isaure et al., in prep.

Table 2. Ca µXANES Results

Treatment	Grain Name	a [1]	Calcite	Vaterite	Aragonite	Amorphous $CaCO_3$	Aqueous Ca^{2+}	Ca oxalate 1 H_2O	Sum	NSS (%) [2]
Zn+Ca	ZnCa3	1.38			97 ± 2				97	0.014 [3]
	ZnCa4	0.12	98 ± 2						98	0.015 [3]
	ZnCa5	0.17	98 ± 2						98	0.021 [3]
Zn	Zn2	0.27			22 ± 10	76 ± 15			97	0.011 [3]
		0.27				77 ± 15		20 ± 15	97	0.016
		0.27				79 ± 15	17 ± 15		96	0.019
		0.42				(excluded)	55 ± 15	45 ± 15	100	0.050
	Zn3		62 ± 5			29 ± 5			91	0.009 [3]
			70 ± 5					22 ± 5	92	0.016
			71 ± 5				21 ± 5		92	0.018

Group	Sample							
Cd+Ca	CdCa2	85 ± 5		13 ± 5			98	0.012 [3]
		87 ± 5				10 ± 5	97	0.014
		89 ± 5			9 ± 5		98	0.015
	CdCa3		77 ± 5	21 ± 7			98	0.031 [3]
			79 ± 5			20 ± 7	99	0.036
			82 ± 5		16 ± 7		98	0.037
	CdCa6	0.38		74 ± 15		25 ± 15	99	0.015 [3]
		0.42		68 ± 15	32 ± 15		100	0.019
		0.28		(excluded)	73 ± 15	25 ± 15	98	0.040
Cd	Cd10	29 ± 7	42 ± 8			25 ± 5	96	0.022 [3]
		25 ± 7	37 ± 8	34 ± 5			96	0.025
		28 ± 7	42 ± 8			26 ± 5	96	0.028

[1] Coefficient of over-absorption. [2] Residual between fit and experimental data $NSS = \Sigma(\mu_{\text{experimental}} - \mu_{\text{fit}})^2 / \Sigma(\mu_{\text{experimental}})^2 \times 100$ in the 4000-4150 eV range, where μ is the normalized absorbance. [3] Fit shown in Fig. 4. The error bars on the percentages correspond to the variation needed to increase NSS by 20%.

Table 3. Summary of the information obtained on each grain[1]

Treatment	Grain Name	Ca Speciation (µXANES Results)[1]	Mineralogy (µXRD Results)	Aspect of the Grain (SEM Results)
Zn+Ca	ZnCa3	100% aragonite	Aragonite, Zn-subst. calcite ($Ca_{0.93}Zn_{0.07}CO_3$)	faceted
	ZnCa4	100% calcite	Zn-subst. calcite ($Ca_{0.87}Zn_{0.13}CO_3$)	faceted
	ZnCa5	100% calcite	Zn-subst. calcite ($Ca_{0.95}Zn_{0.05}CO_3$)	not observed
Zn	Zn2	80% ACC + 20% undetermined	No diffraction peaks	rounded
	Zn3	70% calcite + 30% organic Ca and/or ACC	Zn-subst. calcite ($Ca_{0.89}Zn_{0.11}CO_3$)	not observed
Cd+Ca	CdCa2	90% calcite + 10% organic Ca and/or ACC	Cd-subst. calcite, Cd-subst. vaterite	not observed
	CdCa3	80% vaterite + 20% organic Ca and/or ACC	Cd-subst. vaterite	rounded
	CdCa6	70% ACC + 30% undetermined	No diffraction peaks	not observed
Cd	Cd10	30% calcite + 40% vaterite + 30% organic Ca and/or ACC	Cd-subst. calcite, Cd-subst. vaterite	rounded + faceted

[1] The error bar on the percentages varies from 5 to 15% depending on the species (see Table 2)

Figure Captions

Figure 1: SEM imaging for the grains ZnCa3 (a), ZnCa4 (b) Zn2 (c), CdCa3 (d) and grain Ca3 (e), and EDX analyses were performed on the spots marked by a black cross.

Figure 2: µXRF spectrum (a) one- and two-dimensional µXRD patterns (b) for grain ZnCa5 and Zn3. All XRD peaks were attributed to substituted calcite. The positions of three peaks for pure calcite are indicated by arrows.

Figure 3: Ca K-edge XANES spectra for the reference compounds used in the linear combination fits (a) and zoom on the main peak for aqueous Ca2+, Ca oxalate monohydrate and ACC (b).

Figure 4: Ca K-edge µXANES spectra for the tobacco grains and corresponding linear combination fits. Five spectra (Zn2, CdCa6, ZnCa3, ZnCa5 and ZnCa4) were corrected for over-absorption.
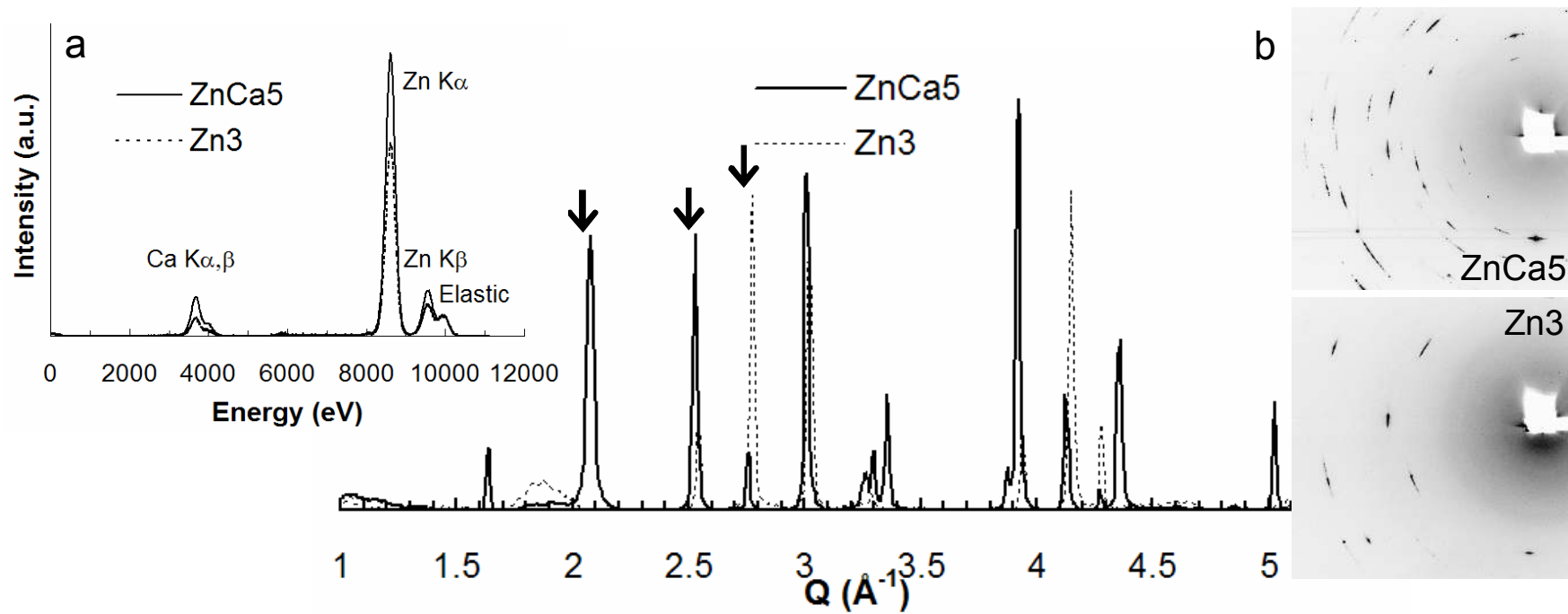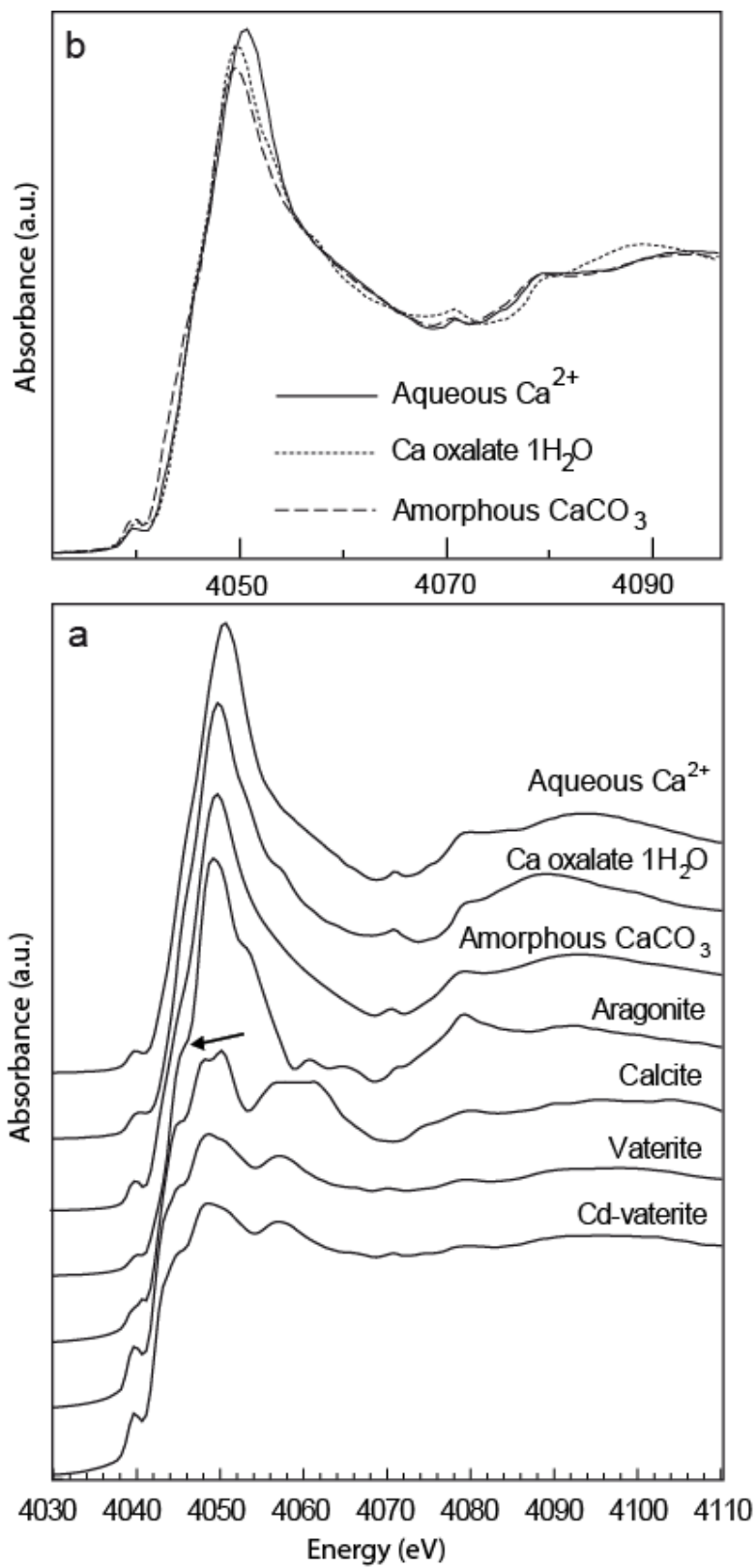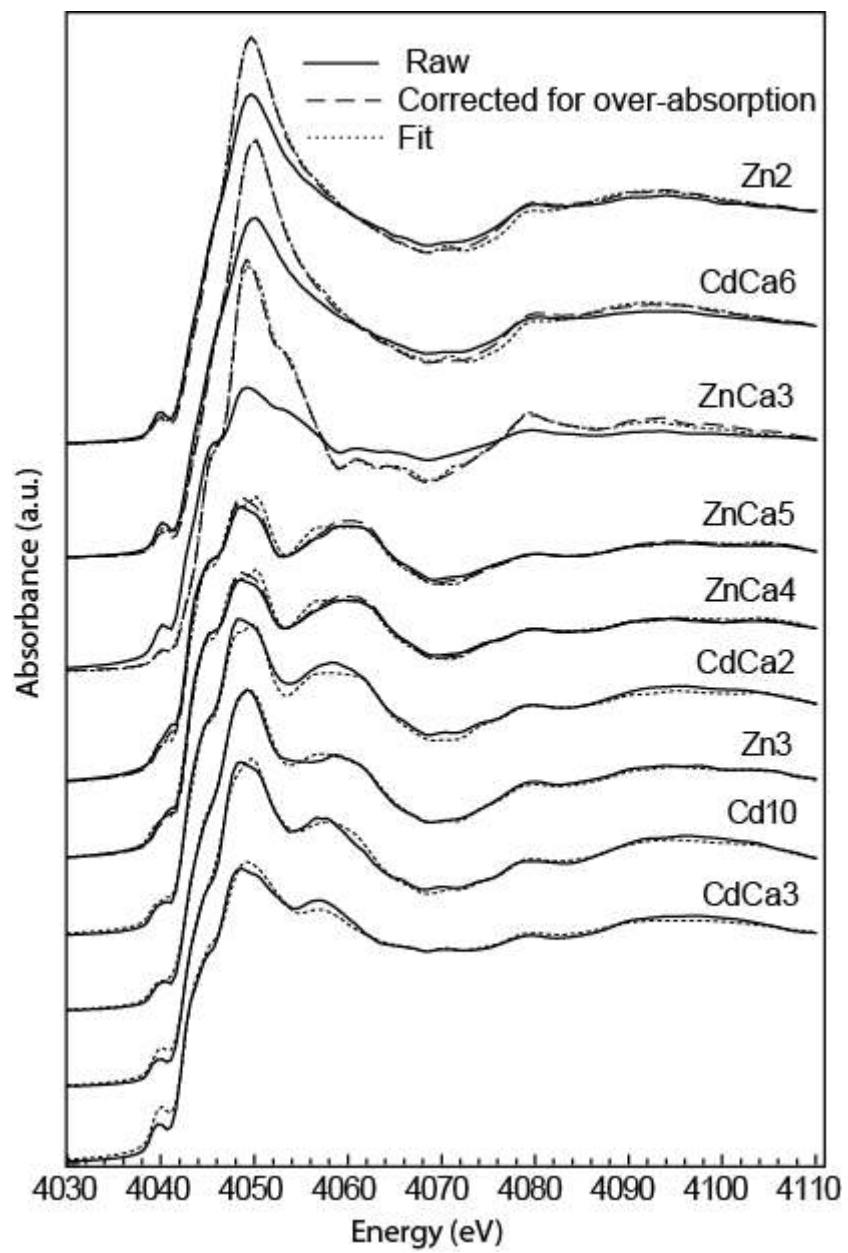
Figure 1

Figure 2

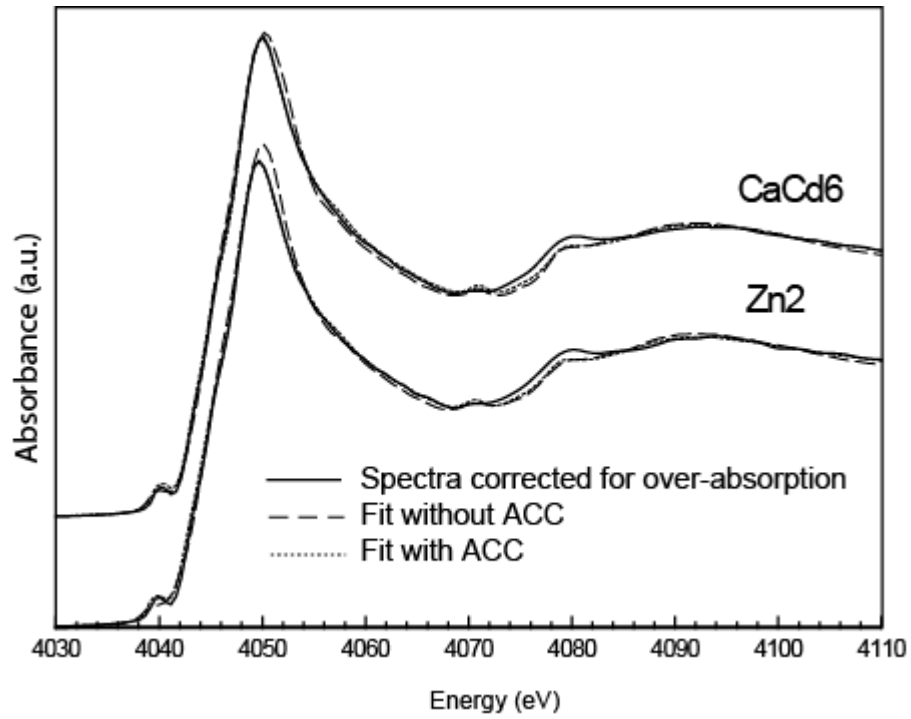Figure 3

Figure 4

Supplemental information

Figure 1: Comparison of the best two-component fits obtained for CaCd6 and Zn2 with and

without ACC.